Antiproton stopping in atomic targets

J. J. Bailey, A. S. Kadyrov, I. B. Abdurakhmanov, D. V. Fursa, and I. Bray
Curtin Institute for Computation and Department of Physics, Astronomy and Medical Radiation Sciences, Curtin University, GPO Box U1987, Perth 6845, Australia

(Received 15 July 2015; published 24 August 2015)

Stopping powers of antiprotons in H, He, Ne, Ar, Kr, and Xe targets are calculated using a semiclassical time-dependent convergent close-coupling method. The helium target is treated using both frozen-core and multiconfiguration approximations. The electron-electron correlation of the target is fully accounted for in both cases. Double ionization and ionization with excitation channels are taken into account using an independent-event model. The Ne, Ar, Kr, and Xe atom wave functions are described in a model of six p-shell electrons above a frozen Hartree-Fock core with only one-electron excitations from the outer p shell allowed. Results obtained for helium in the multiconfiguration treatment are in better agreement with experimental measurements than other theories.

DOI: 10.1103/PhysRevA.92.022707 PACS number(s): 34.10.+x, 34.50.Bw

I. INTRODUCTION

Knowledge of energy losses as particles travel through matter is of fundamental importance in a number of fields, including medical radiation therapy [1], aviation and space exploration [2], and astrophysics [3]. Significant attention is being drawn to the area of antiproton scattering from atoms and molecules due to the development of sources of low-energy antiprotons; see the review of Kirchner and Knudsen [4]. The antiproton decelerator at CERN [5] is extending its extra-low-energy antiproton (ELENA) ring [6] to significantly increase the number of usable or trappable antiprotons, with scattering experiments due to begin in 2017. Interest in the processes occurring during antiproton scattering from atoms and molecules is compounded due to its potential application to radiotherapy and oncology (see, e.g., Refs. [4,7]). Also, the future Facility for Antiproton and Ion Research (FAIR) at GSI has requirements for precise knowledge of the collision mechanisms between antiprotons and various atomic and molecular targets.

With the development of the low-energy antiproton ring (LEAR) facility at CERN, stopping power measurements for antiprotons in He were performed by Agnello *et al.* [8]. They simultaneously measured the spacial coordinates and times of annihilation. Then they solved an inverse problem to obtain the stopping power. Resulting equations are solved numerically using parameters to obtain the best fit to the data. Measurements were performed between 0.5 keV and 1.1 MeV. This data was later reanalyzed by Rizzini *et al.* [9] with emphasis on the Barkas effect [10].

The first quantum-mechanical formulation of energy loss per unit path length, or stopping power, was developed by Bethe [11]. He applied the first Born and dipole approximations and proposed that the stopping power for heavy projectiles traveling through matter at nonrelativistic velocity v is given by

$$-\frac{dE}{dx} = N\frac{4\pi k_e^2 e^4 Z_p^2 Z_t^2}{m_e v^2}\ln\left[\frac{2m_e v^2}{\bar{E}}\right], \qquad (1)$$

where N is the number of target atoms per cubic meter, k_e is the Coulomb constant, e is the elementary charge, m_e is the electron mass, Z_t is the atomic number of the target, $Z_p e$ is the charge of the incident particle, and $\bar{E}$ is the mean excitation energy of the target. Due to the approximations made by Bethe [11], the above formula is applicable only at sufficiently high projectile velocities. However, with the increased interest in heavy projectile interactions with matter due to applications in hadron therapy, it is important that calculations of the stopping power are accurate over the whole energy range, including low energies. With experimental data to compare with, Schiwietz *et al.* [12,13] performed the first theoretical calculations of antiproton stopping power in H and He. They performed calculations using atomic-orbital (AO) close coupling, distorted-wave (DW) Born, and generalized adiabatic-ionization (AI) methods. It was found that the first-order contribution to the stopping power dominates at high velocities with higher-order effects becoming important at intermediate velocities, while near-adiabatic dynamics prevailed in the low-velocity limit. The AO and DW calculations were in agreement above the stopping maximum. The He calculations of Schiwietz *et al.* [12,13] are, in general, not within the experimental uncertainty of Agnello *et al.* [8]. Cabrera-Trujillo *et al.* [14] were the next to contribute from a theoretical perspective. They used electron nuclear dynamics (END) formalism to calculate antiproton energy loss in hydrogen up to 300 keV. The results showed reasonable agreement with the AO method of Schiwietz *et al.* [12,13]. The latest development in the problem comes from Lühr and Saenz [15] who calculated antiproton stopping powers in H and He between 1 keV and 6.4 MeV. They used a semiclassical close-coupling approach to the solution of the time-dependent Schrödinger equation. The radial wave function was expanded in a B-spline basis with the He target described using an effective one-electron treatment. For H, Lühr and Saenz [15] obtained good agreement with the calculations of Schiwietz *et al.* [12,13] and there was reasonable agreement with the calculations of Cabrera-Trujillo *et al.* [14] as well. For He, there was good agreement with the data of Agnello *et al.* [8] above 2 MeV, but disagreement at intermediate and low energies. Lühr and Saenz [15] concluded that this is due to using a one-electron model.

In this paper, we present stopping power calculations of antiprotons in H, He, Ne, Ar, Kr, and Xe. We use a semiclassical time-dependent convergent close-coupling (CCC) method for the calculation of stopping powers. The results presented in this

paper improve upon current theories of Schiwietz *et al.* [12,13] and Lühr and Saenz [15] by employing a multiconfiguration treatment of He which fully accounts for the electron-electron correlation and by taking into account double ionization and ionization with excitation via an independent-event model. The first coupled-channel calculations of scattering cross sections with correlated two-electron dynamics were performed by Hall *et al.* [16,17]; however, their calculations were not applied to stopping powers.

The paper is set out as follows. Section II outlines the method. Section III presents and discusses results. Finally, in Sec. IV, we draw conclusions and discuss future work.

II. THEORY

A. Time-dependent convergent close-coupling method in impact parameter representation

The time-dependent CCC method has been applied to antiproton-impact ionization of molecular hydrogen [18,19] and multielectron targets [20]. Here we briefly describe the method in a general form for single-, two-, and multielectron targets.

The method employs a semiclassical impact-parameter approach, meaning the incident antiproton is treated classically while the target electrons are treated fully quantum mechanically. This semiclassical approximation is valid over all energies considered in this paper. Our calculations are performed in the laboratory frame in which the target is at rest. We assume a straight-line trajectory [$\boldsymbol{R}(t) = \boldsymbol{b} + \boldsymbol{v}t$] for the incident antiproton traveling with velocity $\boldsymbol{v}$, where $\boldsymbol{b}$ is the impact parameter. The nonrelativistic time-dependent Schrödinger equation for the electronic part of the total scattering wave function describing our many-body system is written as

$$H\Psi(t,\boldsymbol{r},\boldsymbol{R}) = i\frac{\partial\Psi(t,\boldsymbol{r},\boldsymbol{R})}{\partial t}, \tag{2}$$

where $\boldsymbol{R}$ is the position vector of the antiproton relative to the target defined above and $\boldsymbol{r}$ collectively denotes the position vectors of all target electrons ($\boldsymbol{r} = \{\boldsymbol{r}_1,...,\boldsymbol{r}_{N_e}\}$). For a hydrogen target, $N_e = 1$, and for a helium target, $N_e = 2$. However, for noble gases, it is not practical to include all target electrons and so we limit ourselves to $N_e = 6$ outer p-shell electrons, with the remaining electrons treated as an inert core. The antiproton-target scattering system has a total Hamiltonian given by

$$H = V + H_t, \tag{3}$$

where H_t is the target atom Hamiltonian and V is the projectile target interaction, written as

$$V = V_0 + \sum_{i=1}^{N_e} V_{0i}. \tag{4}$$

Here, V_{0i} is the interaction of the projectile with the target electrons and V_0 is the interaction of the projectile with the inert core.

The electronic wave function is expanded in terms of a complete set of target pseudostates Φ_α according to

$$\Psi(t,\boldsymbol{r},\boldsymbol{R} = \boldsymbol{b} + \boldsymbol{v}t) = \sum_\alpha A_\alpha(t,\boldsymbol{b})\exp(-i\epsilon_\alpha t)\Phi_\alpha(\boldsymbol{r}), \tag{5}$$

where ϵ_α is the energy of the target electronic state α. The expansion coefficients $A_\alpha(t,\boldsymbol{b})$ define the probability for transitions into electronic bound and continuum states.

Substitution of the expanded total scattering wave function (5) into the time-dependent Schrödinger equation (2) yields a set of coupled-channel differential equations for the time-dependent expansion coefficients $A_\alpha(t,\boldsymbol{b})$,

$$i\frac{dA_\alpha(t,\boldsymbol{b})}{dt} = \sum_\beta A_\beta(t,\boldsymbol{b})\langle\Phi_\alpha|V(t,\boldsymbol{r},\boldsymbol{b})|\Phi_\beta\rangle \times \exp[i(\epsilon_\alpha - \epsilon_\beta)t]. \tag{6}$$

Equation (6) is solved with the initial conditions $A_\alpha(t = -\infty,\boldsymbol{b}) = \delta_{\alpha i}$, as the target is initially in the ground state Φ_i. The probability for transition into some final state f is then

$$p_f(b) = |A_f(t = +\infty,b)|^2. \tag{7}$$

After integrating over impact parameters, one obtains the cross section $\sigma_{\rm fi}$ for the transition from initial state i to final state f.

B. Target structure calculations for H, He, Ne, Ar, Kr, and Xe

For a hydrogen target, the pseudostates in Eq. (5) are written as

$$\Phi_\alpha \equiv \Phi_{nlm}(\boldsymbol{r}) = R_{nl}(r)Y_{lm}(\hat{r}), \tag{8}$$

where

$$R_{nl}(r) = \sum_k B^l_{nk}\xi_{kl}(r). \tag{9}$$

Here, ξ_{kl} is a complete set of basis functions and B^l_{nk} are the expansion coefficients found by diagonalization of the target Hamiltonian ($\langle\Phi_\alpha|H_t|\Phi_\beta\rangle = \epsilon_\alpha\delta_{\alpha\beta}$).

An important feature of the CCC approach is the choice of the basis as a set of orthogonal Laguerre functions,

$$\xi_{kl}(r) = \left[\frac{\lambda_l(k-1)!}{(2l+1+k)!}\right]^{1/2}(\lambda_l r)^{l+1} \times \exp(-\lambda_l r/2)L^{2l+2}_{k-1}(\lambda_l r), \tag{10}$$

where $L^{2l+2}_{k-1}(\lambda_l r)$ are the associated Laguerre polynomials, l is the orbital angular momentum, and index k ranges from 1 to N_l, the maximum number of Laguerre functions. Here, λ_l is the exponential fall-off parameter which is typically chosen to give the most accurate ground state of the target with a minimum number of basis functions. The choice of λ_l should not affect the final result; however, it does affect the speed of convergence. Specific values of λ_l used for each target are given below. This choice of basis allows us to model the whole spectrum of the target atom. As the size of the one-electron basis increases, the low-lying states will converge to the bound states of the target, while the remaining (pseudo)states will provide a representation of the

target atom high-lying bound states and an increasingly dense square-integrable representation of the target continuum.

Full details of the target structure calculations for helium were presented in Fursa and Bray [21] and for noble gas atoms (Ne, Ar, Kr, Xe) in Fursa and Bray [22]. Here we give a short overview only.

Within a nonrelativistic formulation adopted in this paper, the target atom orbital angular momentum l, spin s, and parity π are conserved quantum numbers. For each target symmetry $\{l,s,\pi\}$, the target states are obtained via the configuration-interaction (CI) expansion

$$\Phi_n = \sum_k C_k^n \, \tilde{\Phi}_k, \tag{11}$$

where configurations $\{\tilde{\Phi}_k\}$ are built by orbital angular momentum and spin coupling of one-electron functions. The coefficients C_k^n in the CI expansion (11) are obtained by diagonalization of the target atom Hamiltonian H_t in the basis of configurations $\{\tilde{\Phi}_k\}$.

The one-electron basis is a set of Laguerre functions [23],

$$\phi_\alpha(x) = \phi_\alpha(\boldsymbol{r})\chi(\sigma) = \xi_{k_\alpha l_\alpha}(r) Y_{l_\alpha m_\alpha}(\hat{\boldsymbol{r}})\chi(\sigma), \tag{12}$$

where $\xi_{k_\alpha l_\alpha}$ is the function defined in (10). For helium, the set of configurations is simply antisymmetrized two-electron configurations,

$$|\tilde{\Phi}_k\rangle = \mathcal{A}\,\big|\phi_{\alpha_k},\phi_{\beta_k} : ls\pi\big\rangle. \tag{13}$$

The antisymmetrization operator $\mathcal{A}$ is given by

$$\mathcal{A} = \frac{1}{\sqrt{N_e}}\left(1 - \sum_{i=1}^{N_e-1} P_{iN_e}\right), \tag{14}$$

where P_{ij} is a permutation operator and $N_e = 2$. Note that the $1s$ Laguerre function with $\lambda_0 = 4.0$ is exactly the same as the $1s$ orbital of the He^+ ion. Limiting the set of two-electron configurations to those where one of the electrons occupies the $1s$ He^+ orbital leads to a frozen-core model of helium. Excited states of helium are well described within the frozen-core model. However, the ground-state benefits from a more accurate description which can be readily achieved by allowing for a more general choice of configurations. When several inner orbitals are allowed, we have the multiconfiguration description. We emphasize here that both frozen-core and multiconfiguration descriptions of the target explicitly account for the electron correlation effects.

For the heavier noble gas atoms (Ne, Ar, Kr, Xe), we adopt a model of six p electrons above an inert Hartree-Fock core. Excited states of noble gases are obtained by allowing one-electron excitations from the outer p shell. This model is similar to the frozen-core model of helium. We implement this model in a number of steps. Taking the Ne atom as an example, the first step is to perform the self-consistent Hartree-Fock calculations for the Ne^+ ion that produces $1s$, $2s$, and $2p$ orbitals. Then the quasi-one-electron Hamiltonian of the Ne^{5+} ion is diagonalized in the Laguerre basis (10). This leads to a set of one-electron orbitals from which we drop the $1s$ and $2s$ orbitals and replace the $2p$ orbital with the Hartree-Fock $2p$ orbital. These orbitals are orthogonalized by the Gram-Schmidt procedure to produce the $\{\phi_\alpha\}$ one-electron basis. The configurations are built by angular momentum and spin coupling of the wave function of the $2p^5$ electrons $\psi_c(l_0^{4l_0+1})$ and one-electron functions $\{\phi_\alpha\}$,

$$|\tilde{\Phi}_k\rangle = \mathcal{A}\,\big|\psi_c\big(l_0^{4l_0+1}\big),\phi_{\alpha_k} : ls\pi\big\rangle, \tag{15}$$

where $l_0 = 1$ and the antisymmetrization operator $\mathcal{A}$ is given by (14) with $N_e = 6$.

C. Helium double ionization and ionization with excitation

In this work, we account for double ionization (DI) and ionization with excitation (IE) processes via an independent-event model. In this model, DI and IE are considered a two-step process. The first step is single ionization of He and the second is ionization or excitation of He^+. The probability of the primary electron being ionized and the second electron transitioning from the He^+ ground state to some final state k is the product of the two probabilities. Hence the cross section is

$$\sigma_k^+ = 2\pi \int_0^\infty p_{\rm ion}^{\rm He}(b) p_k^{\rm He^+}(b) b db, \tag{16}$$

where b is the magnitude of the impact parameter $\boldsymbol{b}$, and $p_{\rm ion}^{\rm He}$ is the total ionization probability of helium, which is given by the sum over all probabilities (7) for transitions to positive-energy states.

D. Stopping power

The energy loss per unit path length, or stopping power, is, in general, defined as

$$-\frac{dE}{dx} = N S(E_0), \tag{17}$$

where $S(E_0)$ is referred to as the stopping cross section and is dependent on the incident energy of the projectile, E_0. For heavy projectiles, the total stopping cross section, in the semiclassical approximation, is the sum of two contributions, i.e., the nuclear and the electronic stopping cross sections.

The electronic contribution is the energy losses associated with all excitation and ionization events of the target electrons. In a one-electron target, the electronic stopping cross section is

$$S_{\rm e}(E_0) = \sum_{f=1}^{\infty} (\epsilon_f - \epsilon_i)\sigma_{\rm fi} + \int_0^{E_0+\epsilon_i} (\epsilon - \epsilon_i)\frac{d\sigma}{d\epsilon} d\epsilon, \tag{18}$$

where ϵ_i is the energy of the initial state of the target i, $\sigma_{\rm fi}$ is the cross section for excitation to a state f of energy ϵ_f, and $d\sigma/d\epsilon$ is the single differential cross section for an electron of energy ϵ. Hence one sums over all possible energy losses due to excitation to bound states and integrates over all possible energy losses due to ionization to continuum states.

In the CCC method, we discretize the continuum as described in Sec. II B. Therefore, the integral in Eq. (18) becomes a sum over the total number $N_{\rm T}$ of negative- and positive-energy pseudostates. The electronic stopping cross section is then written as

$$S_{\rm e}(E_0) \approx \sum_{f=1}^{N_{\rm T}} (\epsilon_f - \epsilon_i)\sigma_{\rm fi}. \tag{19}$$

In our calculation of the antiproton-helium electronic stopping cross section, we include energy losses due to excitation and ionization of the inner electron as well. In this instance, we have a second term in our electronic stopping cross section due to these processes,

$$S_e(E_0) \approx \sum_{f=1}^{N_T} (\epsilon_f - \epsilon_i)\sigma_{fi} + \sum_{k=1}^{N'_T} (\epsilon_k - \epsilon^{He^+})\sigma_k^+, \qquad (20)$$

where ϵ^{He^+} is the ground-state energy of He^+, and σ_k^+ is the cross section for the transition of the inner electron to a state k of energy ϵ_k. The process of calculating σ_k^+ is defined by Eq. (16).

The nuclear stopping cross section S_n is due to the kinetic energy transferred to the target atom during elastic and inelastic scattering. Calculations of nuclear stopping were only performed for helium so we could more accurately compare with experiment, which measures all energy-loss contributions at once (electronic plus nuclear). The procedure of calculating nuclear stopping cross sections is, in general, well defined, and given in the Appendix A.

III. RESULTS AND DISCUSSION

A. $\bar{p}$-H

For calculations of electronic stopping cross sections for antiprotons in hydrogen, we find that the maximum orbital angular momentum of the target states, required to reach convergence, is 6, and $N_l = 30 - l$. The exponential fall off λ_l of the basis functions was chosen to be 2. In Fig. 1, we present our result for the antiproton-hydrogen electronic stopping cross section and find good agreement with the theoretical approaches of Schiwietz *et al.* [12,13] (AO), Lühr and Saenz [15], and Cabrera-Trujillo *et al.* [14]. There is currently no experiment to compare with; however, good agreement with other theories validates our method and the associated computer code. Also included is Bethe's formula (1). Our calculations tend toward Bethe's formula at high energies where the latter is applicable. Although the Bethe formula is a high-energy approximation, we have included the full curve to illustrate the extent to which this equation fails at intermediate and low energies. Bethe-type theories are currently relied upon in the field of hadron therapy for depth-dose simulations used in treatment planing. This highlights the potential inaccuracies that can be incurred from the use of such formulas and the need for more accurate calculations.

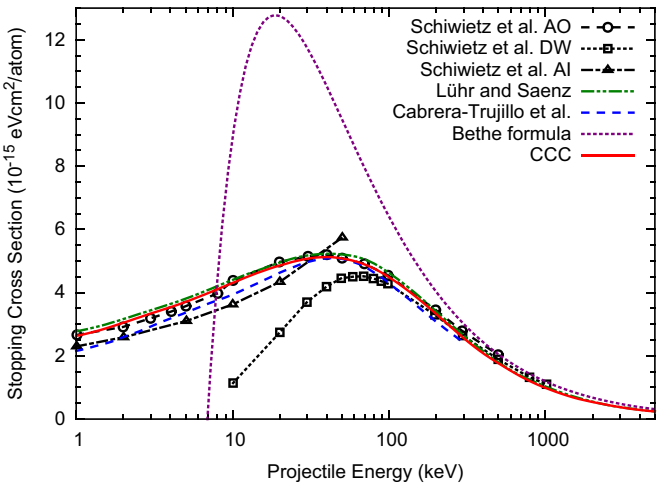

FIG. 1. (Color online) Electronic stopping cross section for antiproton incident on hydrogen. CCC calculations are compared with calculations of Schiwietz *et al.* [12,13], Lühr and Saenz [15], and Cabrera-Trujillo *et al.* [14].

B. $\bar{p}$-He

For our calculations of the electronic stopping cross sections for antiprotons in helium, we find that the maximum orbital angular momentum of the target states required to reach convergence is also 6. However, for He^+, the maximum orbital angular momentum required to achieve the same level of convergence was 4. This reduction in the required maximum orbital angular momentum for He^+ is due to the increase in the binding energy of the target electron. For both He and He^+, sufficient convergence is obtained for $N_l = 20 - l$ with λ_l chosen to be 2. In our multiconfiguration helium calculations, the number of included inner electron orbitals was also increased systematically until convergence was reached. It was found that five s states, four p states, and three d states produced convergent results, while f states and beyond did not give a significant contribution. In a frozen-core approximation, the energy of the helium ground state was obtained to be -23.741 eV. One of the major effects of the multiconfiguration structure model is that it improves the ground state. In our multiconfiguration calculation, we obtain a ground-state ionization energy of 24.540 eV. This is very close to the experimentally measured value of 24.586 eV.

In Fig. 2, we present the result for the antiproton-helium stopping cross section together with the theories of Lühr and Saenz [15] and Schiwietz *et al.* [12,13], and the experimental results of Agnello *et al.* [8]. We use the multiconfiguration

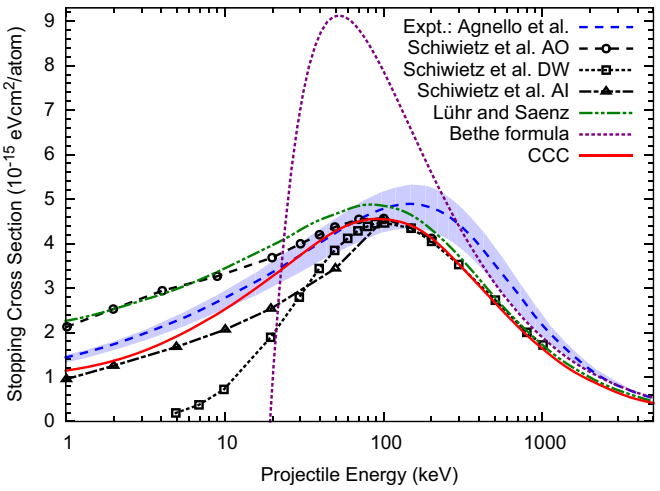

FIG. 2. (Color online) Total stopping cross section for antiproton incident on helium. Included is the experiment of Agnello *et al.* [8], with the shaded region representing the experimental uncertainty. Electronic stopping cross sections of Lühr and Saenz [15] and Schiwietz *et al.* [12,13] are also presented.

representation of helium which, when compared to the frozen-core approach, significantly increases the stopping cross section below the stopping maximum, and slightly reduces it above the maximum. We also take into account double ionization and ionization with excitation via the independent-event model. The nuclear contribution is also added, which makes a noticeable contribution below 5 keV, as discussed later. Our calculations are in agreement with those of Lühr and Saenz [15] above 400 keV and the AO and DW calculations of Schiwietz *et al.* [12,13] above 80 keV, but our calculations appear to systematically underestimate the experiment (except the region from 10 and 150 keV). In this work, we have also evaluated contributions to nuclear stopping from inelastic scattering. This was achieved by summing over the kinetic-energy transfers (A2) corresponding to matrix elements (A4) where Φ_f is no longer the ground-state wave function. However, due to the dominance of the elastic matrix element, these contributions were negligible.

To better understand the reason for the small systematic disagreement, a comment about the experimental data and associated uncertainties is warranted. The experiment of Agnello *et al.* [8] measures the mean annihilation time $\langle t_a \rangle$ and path length R of antiprotons in helium and then simultaneously solves the following two relationships for the total stopping cross section: (i)

$$R = \int_{E_{\rm cap}}^{E_0} \frac{dE}{S(E)}, \tag{21}$$

and (ii)

$$t(E_0) = \int_{E_{\rm cap}}^{E_0} \frac{dE}{vS(E)} = \langle t_a \rangle - \langle t_{\rm cas} \rangle, \tag{22}$$

where v is the antiproton instantaneous velocity, $E_{\rm cap}$ is the antiproton capture energy by the target atom, and $\langle t_{\rm cas} \rangle$ is the mean cascade time. To solve these equations, they make use of a parameterized function for S presented by Andersen and Ziegler [24], where at low energies S is based on the Thomas-Fermi statistical model and is given by $S_l = \alpha E^{\beta}$, and at high energies it is based on Bethe's formula and is given by $S_h = [(243 - 0.375Z_2)Z_2/E]\ln(1 + \gamma/E + 4m_e E/m_{\bar{p}}\bar{E})$. In the intermediate-energy range, an interpolation formula originally proposed by Varelas and Biersack [25] is used, where $1/S = 1/S_l + 1/S_h$. In this formula, α, β, and γ are determined by fitting to their experimentally measured data and were found to be 1.45, 0.29, and 2×10^5, respectively. According to Andersen and Ziegler [24], this particular fitting function has an accuracy of around 10% at 10 keV and 5% at 500 keV. However, the accuracy of the interpolation method in the intermediate-energy range is said to be approximately 20%. This uncertainty is in addition to the shaded region in Fig. 2, which is the limiting behavior determined by the uncertainty in the experimental measurements. The constraints of using a fitting function may be one possible explanation for the small systematic disagreement between our calculations and the experimental data. Furthermore, in the experiment, a beam of antiprotons enters a cylinder containing the helium-gas target. Following a single ionization event, one may have residual He^+ ions within the target gas chamber. To take this into account, we could have added to our calculations in Fig. 2 the stopping cross section associated with antiproton scattering on He^+ multiplied by the probability of He^+ being formed. This could be another possible reason for the disagreement. In terms of uncertainties in our calculations, it must be pointed out that the independent-event model tends to overestimate the double-ionization cross section by approximately 30%. However, since the contribution of double ionization and ionization with excitation processes to the total stopping cross section is small, this leads to about a 2% overestimation at the stopping maximum.

The AO calculations of Schiwietz *et al.* [12,13] and the calculations of Lühr and Saenz [15] are for the electronic stopping cross section. These calculations are in good agreement with each other; however, they significantly overestimate the experimental data below 15 keV. Adding the nuclear stopping cross section would make the disagreement even worse. This overestimation can be attributed to their use of a hydrogenlike description for helium that does not take into account electron correlation effects. The stopping cross section obtained from this model is multiplied by two in order to account for the contribution from both electrons. This demonstrates the importance of using a more detailed structure model if one wishes to obtain more accurate results. The structural improvements over existing theories have allowed us to obtain better agreement with experiment. It is important to emphasize that the CCC results shown in Fig. 2 are based on the cross section for single ionization of helium that is in excellent agreement with experiment.

Individual contributions to the total stopping cross section are presented in Fig. 3. This figure demonstrates the improvement that a multiconfiguration description of the target provides over a frozen-core description at low and intermediate energies. It also shows that energy losses associated with

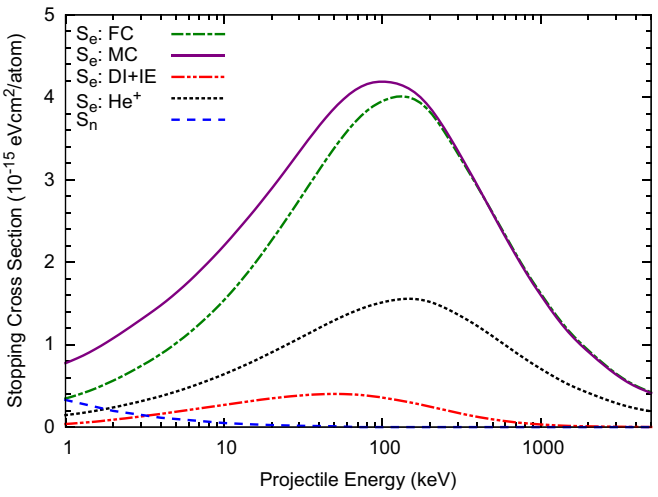

FIG. 3. (Color online) Individual contributions to the antiproton-helium total stopping cross section. FC is the stopping cross section for the primary electron in a frozen-core approximation. Similarly, MC is for the multiconfiguration approximation. DI+IE is the stopping cross section associated with double ionization and ionization with excitation events (obtained using MC treatment). S_n is the nuclear stopping cross section. The stopping cross section for antiprotons in He^+ is also shown.

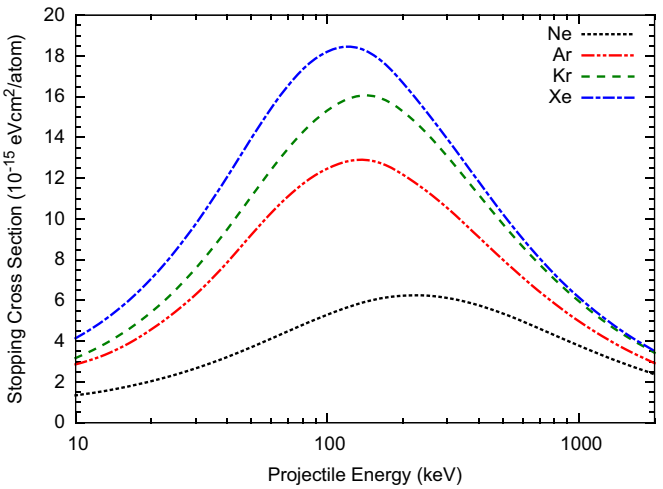

FIG. 4. (Color online) Electronic stopping cross sections due to one-electron transitions from the outer p shell for antiprotons in Ne, Ar, Kr, and Xe.

double ionization and ionization with excitation process make a substantial contribution, as does the nuclear stopping cross section. The stopping cross section for antiprotons in He^+ is also shown.

C. Nobel gas targets

We have also performed antiproton electronic stopping cross-section calculations in the more complex nobel gases of Ne, Ar, Kr, and Xe using the frozen-core treatment with $N_l = 20 - l$ and λ_l chosen to be 2, 2, 2.5, and 3, respectively. For Ne and Ar, the maximum orbital angular momentum of target states used in the calculations were 3 and 5, respectively. For Kr and Xe, the maximum orbital angular momentum of target states was 9. This resulted in the total number of coupled differential equations for the different targets being 803, 1276, and 3475, respectively. To quantitatively assess the accuracy of our structure model for noble gases, we may compare our calculated ionization energies to measured ones. With our frozen-core approximation for Ne, Ar, Kr, and Xe, we obtained ionization energies of 20.57, 14.95, 13.38, and 11.73 eV, respectively, which agree reasonably well with the measured data of 21.56, 16.76, 14.00, and 12.13 eV.

In Fig. 4 we present our electronic stopping cross sections for antiprotons in Ne, Ar, Kr, and Xe. The peak of the stopping cross section increases with the atomic number of the target. This is as expected since the ionization energies decrease with the atomic number of the target and hence the active electron is less tightly bound. We note that these curves are the stopping cross sections associated with the energy losses due to single-electron transitions from the outer p shell.

IV. CONCLUSION

In conclusion, we have applied the CCC method to the calculation of stopping cross sections for antiprotons in H, He, Ne, Ar, Kr, and Xe. We have obtained excellent agreement with existing theories for H and use this as a validation of our approach. For He, we obtained generally better agreement with the experiment of Agnello *et al.* [8] than the other theories due to the use of a multiconfiguration description of the He atom and taking into account double ionization and ionization with excitation via an independent-event model. We also presented calculations of stopping cross sections for antiprotons in Ne, Ar, Kr, and Xe. For the latter, we used a model of six p-shell electrons above a frozen Hartree-Fock core with only one-electron excitations from the outer p shell allowed.

As a next step, we plan to apply the CCC method to calculations of stopping cross sections for antiprotons in molecules. Our ultimate goal is to perform accurate calculations, including rearrangement channels, of protons and carbon ions in biologically relevant molecules for radiation-dose simulations in hadron therapy.

ACKNOWLEDGMENTS

This work was supported by the Australian Research Council, The Pawsey Supercomputer Centre, and the National Computing Infrastructure. A.S.K. acknowledges partial support from the US National Science Foundation under Award No. PHY-1415656.

APPENDIX: THE NUCLEAR STOPPING CROSS SECTION

The nuclear stopping cross section can be modeled as classical scattering from a screened Coulomb potential. It is defined as the integral of the kinetic energy transferred to the target atom over all impact parameters,

$$S_n = 2\pi \int_0^\infty bT(b)db, \tag{A1}$$

where $T(b)$ is the kinetic-energy transfer given by

$$T(b) = 4\mu E_0 \sin^2[\theta(b)/2], \tag{A2}$$

μ is the reduced mass of the system, and θ is the scattering angle defined as

$$\theta(b) = \pi - 2\int_{r_{\min}}^\infty \frac{bdr}{r^2\sqrt{1 - V(r)/E_c - b^2/r^2}}. \tag{A3}$$

Here, $E_c = E_0 M_{He}/(M_{\bar{p}} + M_{He})$ is the center-of-mass energy and $V(r)$ is the screened Coulomb potential. The distance of closest approach $r_{\min}$ is given by the largest zero of the term under the square root.

Calculations of nuclear stopping were performed for helium. For the screened Coulomb potential in Eq. (A3), we use a static potential obtained from

$$V(r) = \langle \Phi_f | -\frac{2}{r} + \frac{1}{|\boldsymbol{r} - \boldsymbol{r}_1|} + \frac{1}{|\boldsymbol{r} - \boldsymbol{r}_2|} | \Phi_i \rangle, \tag{A4}$$

where $\boldsymbol{r}_1$ and $\boldsymbol{r}_2$ are the coordinates of the two electrons in the helium atom, and Φ_i is the ground-state wave function. For elastic scattering, Φ_f is taken to be the ground-state wave function. All other Φ_f wave functions correspond to inelastic scattering. The wave functions are produced in our structure calculations described in Sec. II B.

[1] D. Belkic, *Theory of Heavy Ion Collision Physics in Hadron Therapy*, *Advances in Quantum Chemistry* (Elsevier Science, New York, 2012).
[2] *Shielding Strategies for Human Space Exploration*, edited by J. W. Wilson, J. Miller, A. Konradi, and F. A. Cucinotta, NASA Conf. Pub. No. 3360 (Langley Research Center, Hampton, VA, 1997).
[3] C. Bertulani, Phys. Lett. B **585**, 35 (2004).
[4] T. Kirchner and H. Knudsen, J. Phys. B **44**, 122001 (2011).
[5] "The antiproton decelerator", home.web.cern.ch/about/accelerators/antiproton-decelerator.
[6] "Extra Low Energy Antiproton ring", espace.cern.ch/elena-project.
[7] N. Bassler, J. Alsner, G. Beyer, J. J. DeMarco, M. Doser, D. Hajdukovic, O. Hartley, K. S. Iwamoto, O. Jkel, H. V. Knudsen, S. Kovacevic, S. P. Mller, J. Overgaard, J. B. Petersen, T. D. Solberg, B. S. Srensen, S. Vranjes, B. G. Wouters, and M. H. Holzscheiter, Radiotherapy Oncol. **86**, 14 (2008).
[8] M. Agnello, G. Belli, G. Bendiscioli, A. Bertin, E. Botta, T. Bressani, M. Bruschi, M. Bussa, L. Busso, D. Calvo, B. Cereda, P. Cerello, C. Cicalò, M. Corradini, S. Costa, S. De Castro, A. Donzella, A. Feliciello, L. Ferrero, A. Filippi, V. Filippini, A. Fontana, D. Galli, R. Garfagnini, B. Giacobbe, P. Gianotti, A. Grasso, C. Guaraldo, F. Iazzi, A. Lanaro, E. Rizzini, V. Lucherini, S. Marcello, U. Marconi, A. Masoni, B. Minetti, P. Montagna, M. Morando, F. Nichitiu, D. Panzieri, G. Pauli, M. Piccinini, G. Puddu, E. Rossetto, A. Rotondi, A. Rozhdestvensky, A. Saino, P. Salvini, L. Santi, M. Sapozhnikov, N. Cesari, S. Serci, R. Spighi, P. Temnikov, S. Tessaro, F. Tosello, V. Tretyak, G. Usai, S. Vecchi, L. Venturelli, M. Villa, A. Vitale, A. Zenoni, and A. Zoccoli, Phys. Rev. Lett. **74**, 371 (1995).
[9] E. L. Rizzini, A. Bianconi, M. Bussa, M. Corradini, A. Donzella, M. Leali, L. Venturelli, N. Zurlo, M. Bargiotti, A. Bertin, M. Bruschi, M. Capponi, S. D. Castro, R. Don, L. Fabbri, P. Faccioli, B. Giacobbe, F. Grimaldi, I. Massa, M. Piccinini, N. S. Cesari, R. Spighi, S. Vecchi, M. Villa, A. Vitale, A. Zoccoli, O. Gorchakov, G. Pontecorvo, A. Rozhdestvensky, V. Tretyak, M. Poli, C. Guaraldo, C. Petrascu, F. Balestra, L. Busso, O. Denisov, L. Ferrero, R. Garfagnini, A. Grasso, A. Maggiora, G. Piragino, F. Tosello, G. Zosi, G. Margagliotti, L. Santi, and S. Tessaro, Phys. Lett. B **599**, 190 (2004).
[10] W. H. Barkas, J. N. Dyer, and H. H. Heckman, Phys. Rev. Lett. **11**, 26 (1963).
[11] H. Bethe, Ann. Phys. **397**, 325 (1930).
[12] G. Schiwietz, U. Wille, R. D. Muiño, P. Fainstein, and P. L. Grande, Nucl. Instrum. Methods Phys. Res. B **115**, 106 (1996).
[13] G. Schiwietz, U. Wille, R. D. Muiño, P. D. Fainstein, and P. L. Grande, J. Phys. B **29**, 307 (1996).
[14] R. Cabrera-Trujillo, J. R. Sabin, Y. Öhrn, and E. Deumens, Phys. Rev. A **71**, 012901 (2005).
[15] A. Lühr and A. Saenz, Phys. Rev. A **79**, 042901 (2009).
[16] K. A. Hall, J. F. Reading, and A. L. Ford, J. Phys. B **27**, 5257 (1994).
[17] K. A. Hall, J. F. Reading, and A. L. Ford, J. Phys. B **29**, 6123 (1996).
[18] I. B. Abdurakhmanov, A. S. Kadyrov, D. V. Fursa, and I. Bray, Phys. Rev. Lett. **111**, 173201 (2013).
[19] I. B. Abdurakhmanov, A. S. Kadyrov, D. V. Fursa, S. K. Avazbaev, and I. Bray, Phys. Rev. A **89**, 042706 (2014).
[20] I. B. Abdurakhmanov, A. S. Kadyrov, D. V. Fursa, S. K. Avazbaev, J. J. Bailey, and I. Bray, Phys. Rev. A **91**, 022712 (2015).
[21] D. V. Fursa and I. Bray, Phys. Rev. A **52**, 1279 (1995).
[22] D. V. Fursa and I. Bray, New J. Phys. **14**, 035002 (2012).
[23] I. Bray, Phys. Rev. A **49**, 1066 (1994).
[24] H. Andersen and J. Ziegler, *Hydrogen Stopping Powers and Ranges in All Elements*, *Stopping and Ranges of Ions in Matter* (Pergamon, New York, 1977).
[25] C. Varelas and J. Biersack, Nucl. Instrum. Methods **79**, 213 (1970).